3-D Capabilities for GPS Transceiver Arrays

Masayoshi Matsuoka, Edward A. LeMaster, Stephen M. Rock, *Stanford University*

BIOGRAPHY

Masayoshi Matsuoka is a Ph.D. candidate in the Department of Aeronautics and Astronautics at Stanford University. He received his B.S. and M.S. in Aeronautics and Astronautics from the University of Tokyo in 2000. His research focuses on developing advanced navigation systems for future robotic planetary explorations.

Edward A. LeMaster is a Senior Controls Engineer at the Lockheed Martin Advanced Technology Center. He received his B.S. in Aeronautical and Astronautical Engineering from the University of Washington in 1995 and his M.S. from Stanford University in 1996. Dr. LeMaster completed his Ph.D. at the Aerospace Robotics Laboratory at Stanford in 2002, where he worked on applying GPS pseudolites to robotic systems, specifically as an aid to Mars rover navigation and cooperative task execution. Previously, Dr. LeMaster developed an integrated GPS/computer-vision navigation system for the Stanford HUMMINGBIRD autonomous helicopter.

Stephen M. Rock is an Associate Professor of Aeronautics and Astronautics at Stanford University. He received his S.B. and S.M. in Mechanical Engineering from MIT in 1972 and Ph.D. in Applied Mechanics from Stanford University in 1978. Dr. Rock joined the Stanford faculty in 1988 where he teaches courses in dynamics and control and pursues research in developing and applying advanced control techniques for vehicle and robot applications. Prior to joining the Stanford faculty, Dr. Rock led the advanced controls group of Systems Control Technology.

ABSTRACT

The Aerospace Robotics Laboratory (ARL) at Stanford University has developed a GPS pseudolite-based local-area navigation system for Mars rovers, called a Self-Calibrating Pseudolite Array (SCPA) [1]. By utilizing bi-directional ranging GPS transceivers (incorporating separate pseudolites and GPS receivers) scattered over a local area, the SCPA is capable of drift-free centimeter-level localization of the rover with respect to the local array. Relative motion between the rover and the ground-based transceivers is sufficient to determine the precise configuration of the array, eliminating the need for *a priori* position information or precise placement of the devices.

This paper extends the previous work to examine the three-dimensional navigation capability of the SCPA for mobile vehicles moving out of the plane of the ground-based GPS transceiver array. Simulation results show that the SCPA self-calibration algorithm can be applied to 3-D positioning, successfully resolving the relative 3-D trajectories of mobile vehicles with respect to the ground-based array. This paper also presents field demonstrations that validate the actual 3-D positioning capability of the SCPA by using a mobile aerial unit (balloon) equipped with a GPS transceiver. These experimental results show that the 3D-SCPA is able to resolve both the balloon and rover 3-D trajectories relative to the ground-based array to centimeter-level accuracy, starting with no *a priori* knowledge of the ground-based pseudolite locations.

INTRODUCTION

Mobility is a key requirement for future Mars surface exploration missions. Many robotic tasks, such as area surveys, sample collection, and life detection, must be performed autonomously, and this will require greatly enhanced sensing capabilities for navigation over the uncertain and potentially hostile Martian terrain. A GPS-like drift-free RF positioning system would be highly beneficial as an augmentation to conventional rover positioning systems based on odometers and inertial sensors. Although it is possible to construct a GPS-like local-area navigation system without a complete satellite constellation by deploying pseudolites on the Martian surface, it would be extremely difficult to place pseudolites on Mars at precisely known locations relative to each other.

The SCPA overcomes this difficulty through a self-calibration process: First several static transceiver

beacons are deployed at unknown locations. Next, a rover equipped with a transceiver drives around the deployed beacon arrays until enough geometry change has accumulated to resolve all of the biases and integers in the carrier phase measurements for carrier-level positioning. By batch-processing the sampled data during the rover motions, the SCPA can determine both the deployed transceiver locations and the rover trajectories during the self-calibration process. The two-dimensional navigation and self-calibration capability of the SCPA (a planar array with three static transceivers and one mobile unit with planar motion) has been validated previously in field trials performed at NASA Ames Research Center with the K9 Mars Rover [2].

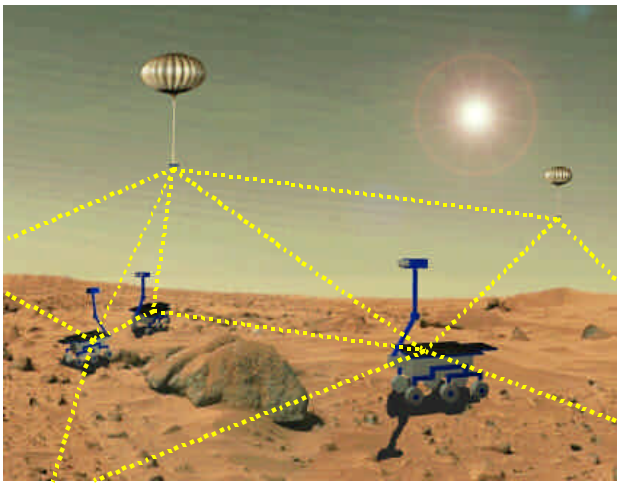

Figure 1: Mars SCPA

This paper extends the previous work to examine the 3-D navigation capability of the SCPA by utilizing GPS transceiver arrays. Possible target applications of the 3D-SCPA include navigation and guidance for aerial vehicles such as balloons and airplanes. These aerial vehicles could be the next generation of Mars exploration platforms, and could perform scientific surveys over much broader areas than rovers. The 3D-SCPA could also be useful as a guidance aid when landing vehicles at precise locations of interest.

To analyze further the 3-D navigation capability of the SCPA, this paper compares several possible configurations in terms of the number of GPS transceivers, the array geometry, and the amount of relative rover-balloon motion required to resolve the carrier phase integer biases. This paper also discusses the potential advantage of sensor fusion with other dissimilar sensors such as altimeters. Practical implementation issues such as robustness in the bi-directional ranging process and possible antenna configurations are also addressed, followed by a description of successful field demonstrations of the three-dimensional self-calibration.

GPS TRANSCEIVER AND SELF-CALIBRATION

Bi-directional Ranging

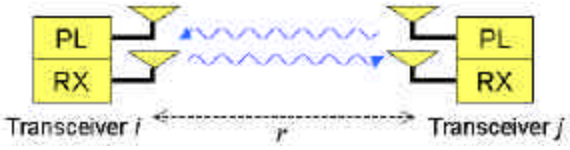

Figure 2: Bi-directional ranging

A GPS transceiver is a cooperating (but potentially separate) pair of devices consisting of a pseudolite and a GPS receiver. By collocating both transmitting and receiving antennas, four phase measurements (two cross-tracking (f_i^j, f_j^i) and two self-tracking (f_i^i, f_j^j)) are obtained between a pair of GPS transceivers at each sampling instant (Equation 1).

$$\begin{bmatrix} f_i^i \\ f_i^j \\ f_j^j \\ f_j^i \end{bmatrix} = \begin{bmatrix} t^i \\ t^j \\ t^j \\ t^i \end{bmatrix} + \begin{bmatrix} t_i \\ t_j \\ t_j \\ t_j \end{bmatrix} + \begin{bmatrix} 0 \\ r_{i-j} \\ 0 \\ r_{i-j} \end{bmatrix} + \begin{bmatrix} 0 \\ N \\ 0 \\ N \end{bmatrix} \quad (1)$$

where

r_{i-j} : range between XCVR i and j

t^i : pseudolite i clock bias

t_i : receiver i clock bias

f_i^j : measurement of carrier phase from pseudolite j at receiver i

N : integer bias

By taking a double-difference combination of the above four measurements, the bi-directional range and relative clock biases between two GPS transceivers are formulated as follows:

$$\begin{bmatrix} r_{i-j} \\ t^i - t^j \\ t_i - t_j \end{bmatrix} = \frac{1}{2}\begin{bmatrix} -1 & 1 & -1 & 1 \\ 1 & -1 & -1 & 1 \\ 1 & 1 & -1 & -1 \end{bmatrix}\begin{bmatrix} f_i^i \\ f_i^j \\ f_j^j \\ f_j^i \end{bmatrix} + \begin{bmatrix} N \\ 0 \\ 0 \end{bmatrix} \quad (2)$$

Figure 3 shows typical accuracy of code- and carrier-range obtained by an actual pair of GPS transceivers (IntegriNautics pseudolites and CMC AllStar receivers). The position of the one transceiver was fixed at 0 m and the other was moved from 20 m to 100 m in 20 m increments. Using code range, an RMS error of 2.51 m

and a maximum error of 4.91 m were observed. The corresponding delta-range using carrier phase measurements has cm-level accuracy. The integer bias of the carrier phase range measurements was initialized at the known starting position (20 m).

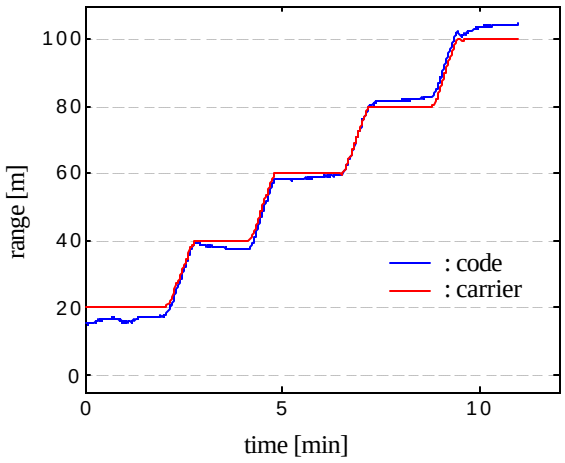

Figure 3: Accuracy of bi-directional ranging

Self-Calibration Algorithms

The basic mode of operation of the SCPA algorithm is as follows: After deployment of transceiver arrays at unknown locations, determination of array geometry and the locations of mobile units starts with a coarse initial estimate obtained by triangulation of code ranges between transceiver pairs. Then, carrier phase measurements are collected during motions of mobile units until enough relative geometry change is accumulated to resolve the integer biases in the carrier phase measurements. By batch-processing the sampled data, the SCPA is able to determine the array locations and the trajectories of mobile units to cm-level accuracy data via a non-linear iterative least square (ILS). The detailed description of the SCPA algorithm is in [1].

ARRAY CONFIGURATIONS

Number of Transceivers for Array Self-Calibration

To achieve enough observability for the batch self-calibration process to determine the transceiver locations, data samples must be collected until the number of range measurements becomes greater than the number of unknowns (Equation 3). The number of constant unknowns includes the initial locations of mobile transceivers and the locations of stationary transceivers (minus the fixed constraints from either the 2-D or 3-D coordinate-frame definition).

$$\begin{cases} \left(M \cdot N + {}_{M}C_{2}\right) \cdot K \geq M \cdot D \cdot K + C \\ C = N \cdot D + M \cdot D - D\ (D+1)/2 \end{cases} \qquad (3)$$

where

N : number of stationary XCVRs
M : number of mobile XCVRs
K : number of data samples
C : number of coordinate constraints
D : overall dimension of the array (2-D or 3-D)

Table 1 shows the minimum number of GPS transceivers required for the array self-calibration, depending on the number of mobile transceivers available in both the 2-D or 3-D arrays. For example, in order to implement the self-calibration using motion by one mobile transceiver, at least three stationary transceivers are required for a 2-D array; four are needed for 3-D. The boxes are shaded when M >= 4 because at least two transceivers (three for 3-D) must be stationary in order to solve for the absolute transceiver locations with respect to a fixed coordinate system. In the extreme case, however, all of the transceivers can be mobile when M >= 7 for 2-D (M >= 8 for 3-D) if only the relative shape of the array is of interest.

# of mobile XCRVs	min. # of stationary XCVRs	
	2-D	3-D
M = 1	3	4
M = 2	2	3
M = 3	2	3
M = 4	1	2
M = 5	1	2
M = 6	1	1
M = 7	0	1
M 8	0	0

Table 1: Minimum # of XCVRs for array self-calibration

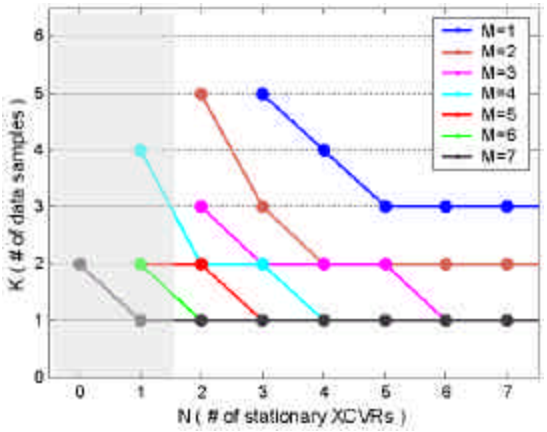

Figure 4: Minimum # of data samples (2-D)

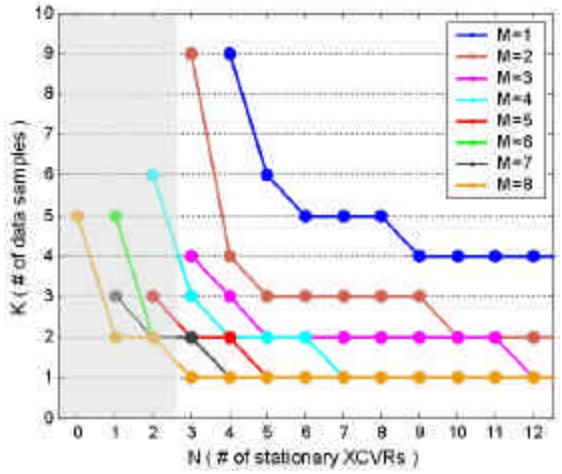

Figure 5: Minimum # of data samples (3-D)

The minimum number of necessary data samples is also a function of the number of transceivers in the array (Figures 4 and 5). For instance, in the case of 3-D positioning using one mobile transceiver with four stationary transceivers, at least nine data samples must be collected during the batch process in order to resolve all the unknowns, assuming the relative motions provide enough observability of the states of interest.

Mobile Arrays

The "stationary" transceivers are not required to be stationary at all times during the self-calibration process. As long as the minimum number of stationary transceivers listed in Table 1 is instantaneously satisfied, each transceiver can switch its state to be either mobile or stationary. For example, the self-calibration still works in the case when each of four transceivers moves separately at different stages of the process. Figure 6 shows that the aggregate motion by all four transceivers achieves enough geometry change to self-calibrate both the trajectories and the unknown initial array locations. In Figure 6, the self-calibration results (red) almost match the true locations (blue). The RMS errors are 14.13 m before self-calibration and 0.01 m after self-calibration. In this simulation, uncertainty of 0.01 m is included to the carrier phase range measurements.

This leads to the concept of mobile arrays in which the arrays move as a whole from one location to another [3], enabling drift-free navigation over longer traverses on the Martian surface by conserving relative position information with respect to their original array locations. The capabilities of mobile arrays will be further investigated in future work.

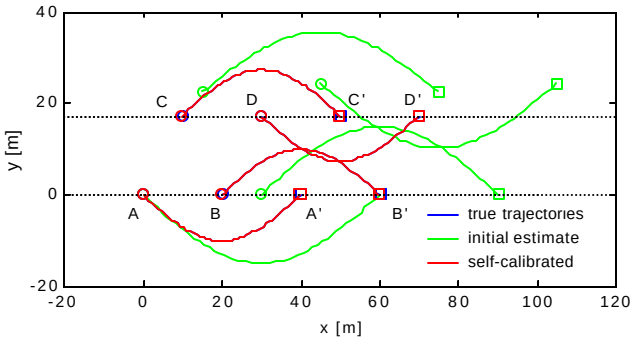

unknowns	$x_B(0), x_C(0), y_C(0), x_D(0), y_D(0), x_A(k), y_A(k)$ $x_B(k), y_B(k), x_C(k), y_C(k), x_D(k), y_D(k)$

Figure 6: Self-calibration on mobile arrays

RX-only Mobile Units

Although theoretically an infinite number of users with mobile transceivers can operate within a given transceiver array, more transceivers aggravate the near-far problem even with pulsed pseudolites (the available pulsing slots get narrower). In order to minimize the RF signal interference, it is desirable to keep the number of signal sources (pseudolites) in the system to a minimum.

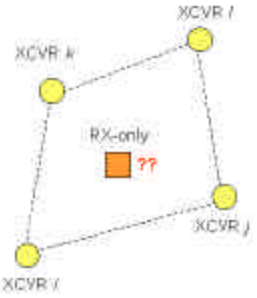

Figure 7: Self-calibration by RX-only unit

For a receiver-only unit to operate within a transceiver array (Figure 7), the receiver clock biases at every sampling instant must be solved as additional unknowns, since they do not cancel out as in bi-directional formulations (Equation 2). All of the unknowns including these receiver clock biases can be self-calibrated by adding one more stationary transceiver to the number shown in Table 1. For an array with one mobile receiver-only unit to self-calibrate, at least four stationary transceivers for 2-D (five for 3-D) are required in the array.

ARRAY GEOMETRY

DOP Analysis

The accuracy of the position estimate depends on both the accuracy of the range measurement and array geometry: the latter factor can be measured by the Dilution of Precision (DOP) [4]. Figure 8 shows the DOP contour maps for a four-transceiver square array with a known 50 m baseline. As the altitude gets higher, the HDOP gets worse and the VDOP gets better, which results in an optimal PDOP at $(x,y,z)=(25,25,25)$. The VDOP at $z=0$ is infinite, which means that vertical positions are unobservable on the $z=0$ plane of planar arrays. Simply having an out-of-plane stationary transceiver makes altitude observable, as is shown in Figure 9.

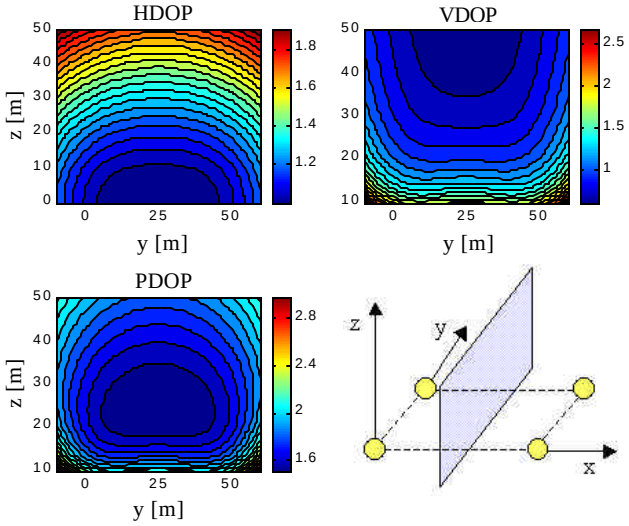

Figure 8: DOP maps for square planar arrays

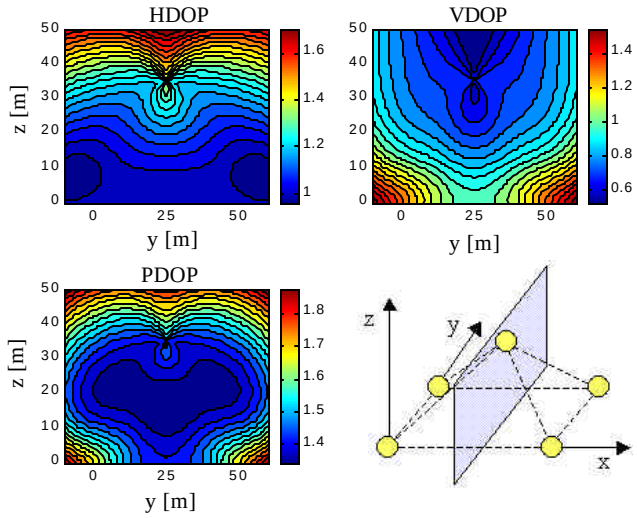

Figure 9: DOP maps for pyramidal arrays

MOTIONS FOR 3-D SELF-CALIBRATIONS

Satisfying the conditions of Equation 3 alone is not sufficient for the successful self-calibration due to uncertainty in the range measurements. As a practical matter, high observability can be achieved by taking data samples at well-spread locations over the arrays to avoid singularities among the collected set of measurement equations. This section examines two different types of 3D-SCPA configurations to investigate how great of a geometry change is required for successful 3-D self-calibration, using either ground motions by a rover or aerial motions by a balloon.

Rover Motions

Configuration Type A illustrated in Figure 10 consists of an array with two mobile transceivers (a rover and a balloon) and three stationary transceivers, in which the rover moves on the ground while the tethered balloon is passively floating in the air above the ground-based array without any large-scale self-induced motion.

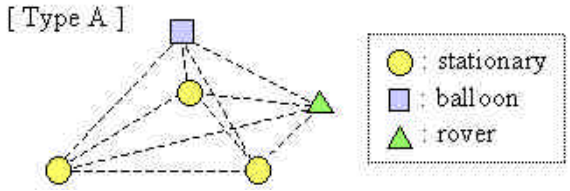

Figure 10: 3D-SCPA configurations (Type A)

The relative motion of the rover provides the geometry change required for the self-calibration process. Simulation results[1] (Figure 11) show that the 2-D rover ground motions (with $z_D=0$ known) successfully self-calibrate all of the unknowns: the stationary transceiver locations, 2-D rover trajectory, and 3-D balloon trajectory to the centimeter-level accuracy locations. In Figure 11, the self-calibration results (red) almost match with the true locations (blue). The RMS errors are 2.43 m in the initial estimates and 0.01 m in the self-calibrated solutions. (Uncertainty of 0.01 m is included in the carrier phase range measurements in all the self-calibration simulations shown in this paper.)

[1] The line colors of the self-calibration plots in this paper are defined as follows unless otherwise mentioned:
— : true
— : initial estimate
— : self-calibrated

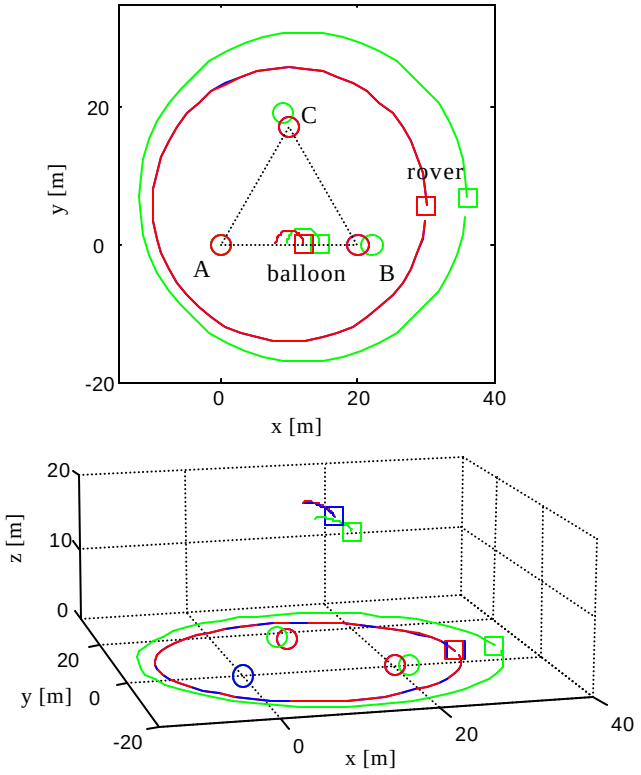

unknowns	$x_B, x_C, y_C, x_{rover}(k), y_{rover}(k),$ $x_{balloon}(k), y_{balloon}(k), z_{balloon}(k)$

Figure 11: Self-calibration of Type A array by rover motion (with $z_{rover} = 0$ known)

Balloon Motions

Configuration Type B in Figure 12 shows an array with one mobile and four stationary transceivers. The ground-based transceivers are placed in a square with 50 m baselines. As illustrated in Figure 12, one of the ground-based transceivers must be placed out of the plane of the rest of the other ground-based transceivers; otherwise vertical positions are unobservable on the plane because of the infinite VDOP at z = 0. A balloon equipped with a GPS transceiver flies above the ground-based stationary array in order to resolve both the unknown locations of the stationary transceivers and the unknown balloon trajectory.

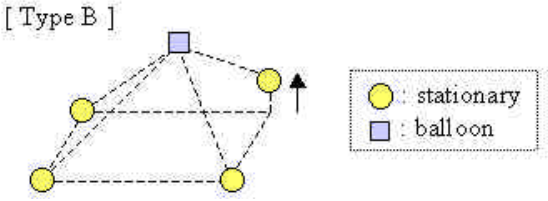

Figure 12: 3D-SCPA configurations (Type B)

Figure 13 shows the simulation result of the self-calibration for the array of Type B configuration using the balloon motion. In this simulation, the fourth stationary transceiver was raised 2 m (with z_D unknown) above the plane of the rest of the stationary transceivers to avoid unobservability of planar arrays. Otherwise, the self-calibration process never converges to the correct answers. In addition, a certain amount of up-down balloon motion is required to overcome vertical observabilty. In Figure 13, the self-calibration results (red) almost match the true locations (blue). The RMS errors are 4.99 m for the initial estimates and 0.38 m for the self-calibrated solutions.

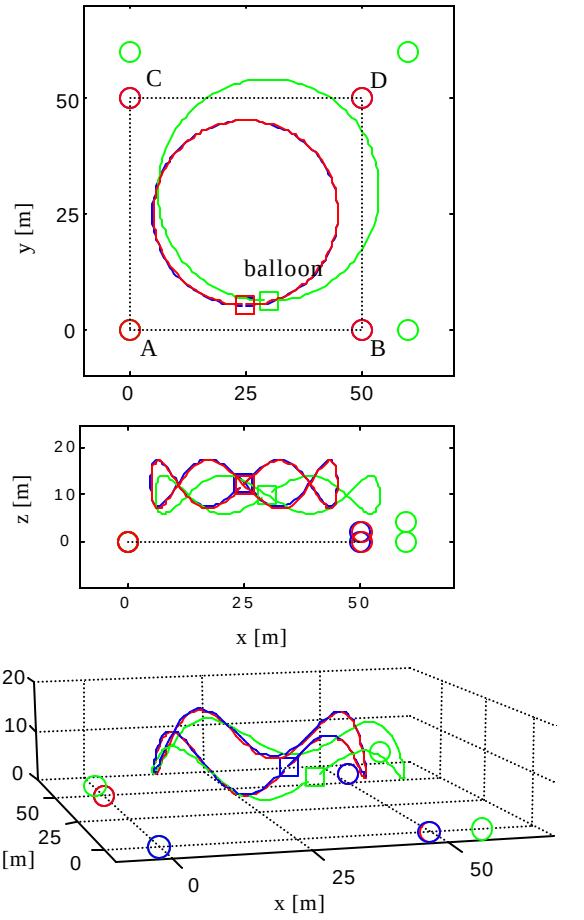

unknowns	$x_B, x_C, y_C, x_D, y_D, z_D, x_{balloon}(k), y_{balloon}(k), z_{balloon}(k)$

Figure 13: Self-calibrations of Type B array by 3-D balloon motion

USE OF ALTIMETER

If an out-of-plane stationary transceiver is not available, fusion with additional sensors, such as altimeter measurements, could possibly mitigate the difficulty by

explicitly providing vertical position information in order to compensate the poor geometry of planar arrays (Figure 14).

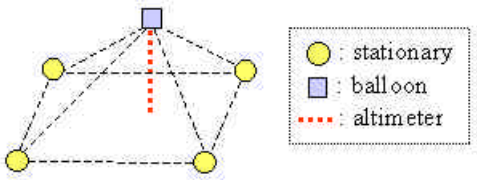

Figure 14: Balloon with altimeter over planar array

Figure 15 shows the successful result for the self-calibration of a planar array with altimeter measurements, in which the balloon moves near z = 0. The altitude of the balloon unit $z_{balloon}$ is simply given as a known value from altimeter measurements. Uncertainty of 0.5 m (the typical accuracy of commercial laser altimeters) is included in the altimeter measurements in this simulation. In Figure 15, the self-calibration results (red) almost match the true locations (blue). The RMS errors are 9.19 m for the initial estimates and 0.01 m for the self-calibrated solutions.

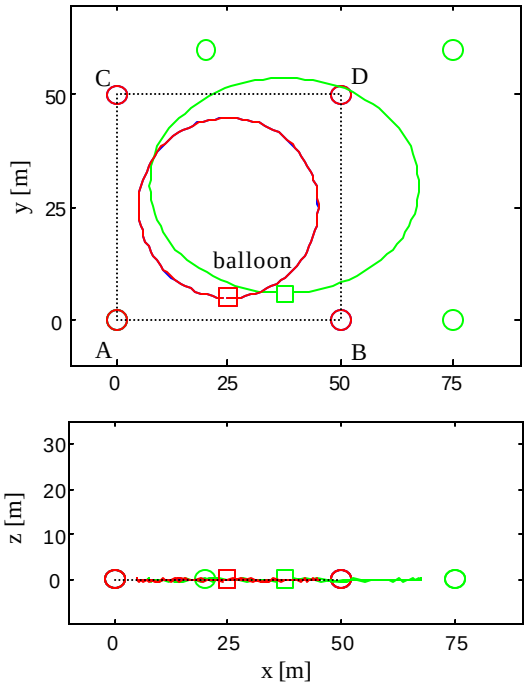

unknowns	$x_B, x_C, y_C, x_D, y_D, x_{balloon}(k), y_{balloon}(k)$

Figure 15: Self-calibration of planar array with altimeter (balloon motion at z = 0 m)

However, if the balloon altitude goes higher, the self-calibration results are shifted from the true locations. Figure 16 shows the result of the same simulation but with the balloon motion at z = 25 m. The RMS errors are 9.19 m for the initial estimates and 1.39 m for the self-calibrated solutions.

This is explained as follows: The planar array has the infinite VDOP at z = 0 plane, which means that the vertical uncertainty of the altimeter near z = 0 has no effect on the horizontal array locations in the self-calibration process. On the other hand, as the balloon altitude goes higher, the self-calibration process becomes more sensitive to the uncertainty of the altimeter measurements, which causes it to converge to horizontally-shifted locations. Therefore, although fusing altimeter measurements greatly helps the self-calibration process in the case of poor array geometry such as planar arrays, the altimeter measurements must be accurate enough to overcome its horizontal sensitivity at higher altitude.

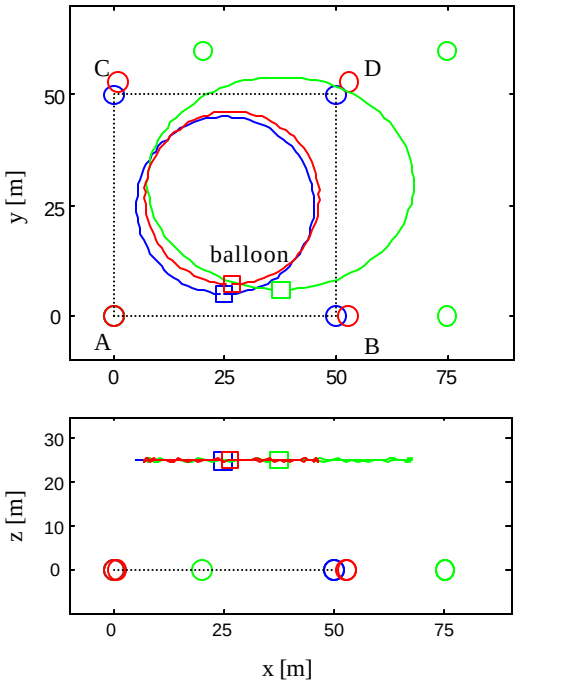

unknowns	$x_B, x_C, y_C, x_D, y_D, x_{balloon}(k), y_{balloon}(k)$

Figure 16: Self-calibration of planar array with altimeter (balloon motion at z = 25 m)

PRACTICAL ISSUES

This section describes some practical issues addressed especially on the 3-D array field demonstrations: robustness of transceiver ranging and possible configurations of collocated pair of antennas.

Signal Drops

To implement the self-calibration by using bi-directional ranging, all four signals (Equation 1) between each pair of transceivers must be continuously tracked until motions by mobile units create enough array geometry change to resolve all the unknowns. However, it is difficult to maintain all the signal locks during entire trajectories [5], particularly when more intensive motions are necessary such as in larger arrays or 3-D arrays. In fact, it is likely that a couple of signal drops will be observed especially in cross-tracking. If any signal drop occurs before the self-calibration is finished, the process must be restarted again . Thus, a new alternative way of transceiver ranging is formulated below to describe how to recover from those fatal signal drops in the actual implementation of the self-calibrations.

Suppose that one of the cross-tracking measurement is dropped out (hence f_i^j is not available in Equation 1), the range between transceiver *i* and *j* is expressed as a function of phase measurements and clock biases, which can not be cancelled out:

$$r_{i-j} = \frac{1}{2}\{(t^i - t^j) - (t_i - t_j)\} + \frac{1}{2}[-1 \quad 2 \quad -1]\begin{bmatrix} f_i^i \\ f_i^j \\ f_j^j \end{bmatrix} \qquad (4)$$

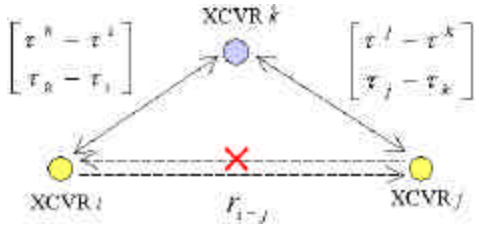

Figure 16: Use of 3rd XCVR

If an additional third transceiver *k* is being tracked bi-directionally with both the transceivers *i* and *j* as illustrated in Figure 16, however, the range r_{i-j} can still be obtained as those clock biases between the transceivers *i* and *j* are solved through the third transceiver *k* clock biases.

$$\begin{cases} t^i - t^j = -(t^k - t^i) - (t^j - t^k) \\ t_i - t_j = -(t_k - t_i) - (t_j - t_k) \end{cases} \qquad (5)$$

Figure 17 shows the stationary range test for the normal bi-directional ranging and for the ranging recovered through the third transceiver without using f_i^j. Although the range solution by way of the third transceiver is a little noisier and has a small bias compared to the normal bi-directional solution, the difference between them is so negligible that this new formulation is a useful way of recovery in case of signal drops on cross-tracking. As it turned out, this method greatly improved the robustness of the actual implementation and was applied several times to recover ranges when there were signal drops during the self-calibration process.

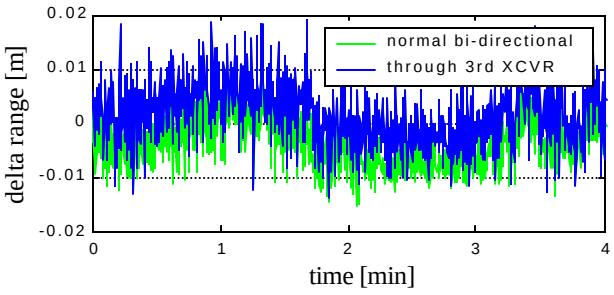

Figure 17: Range recovery through 3rd XCVR

Cycle Windups

When a circular polarization antenna is rotated in 360 degree as illustrated in Figure 18, a cycle counter of carrier phase in a receiver miscounts one cycle less or more (depending on its direction), which results in a range shift by one wave length, known as “cycle windups” [6].

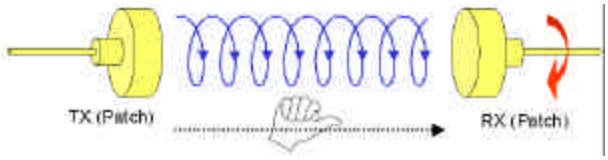

Figure 18: Effect of RHCP antenna rotation

Figure 19 shows the cycle windups actually observed in the bi-directional ranging. One pair of TX-RX antennas was fixed and the other was rotated horizontally by 360 degree without changing the range between the two transceivers. While the dipole-dipole pair had no cycle windup (top), the dipole-patch pair had a half-wavelength shift (middle) due to the one cycle windup divided by 2 (See Equation 2). The patch-patch pair had a whole wavelength shift with two cycle windups divided by 2 (bottom).

Dipole-dipole antenna configurations have been used in the previous field trials [2] to provide horizontal signal coverage over the 2-D planar array, as well as to avoid these cycle windups due to relative motions among transceiver units. However, since the dipole antennas had some difficulties in tracking signals among the 3-D spaced transceivers, RHCP patch antennas were used to achieve better receptions over the 3-D arrays. Therefore, the accuracy degradations due to the effect of antenna

rotation must be taken into account in the following field test results.

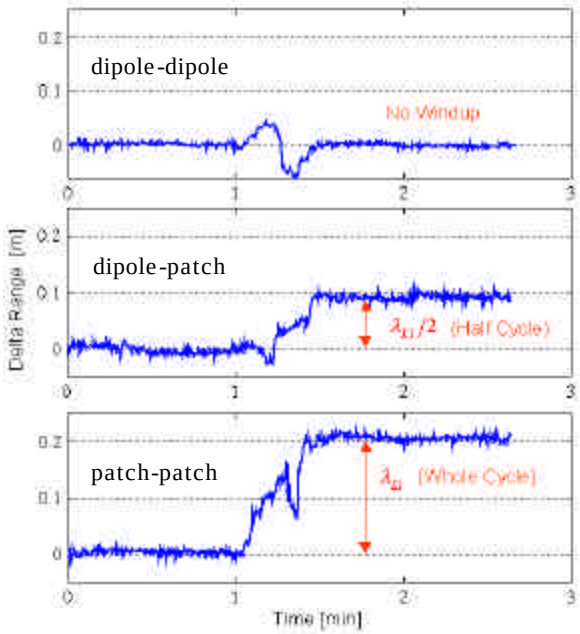

Figure 19: Cycle windups in bi-directional ranging

FIELD DEMONSTRATION

This section presents the result from field trials conducted at Stanford University on July 2002 in order to validate the actual 3-D positioning capabilities of 3D-SCPA using GPS transceiver arrays.

Figure 20: Field trials at Roble Field, Stanford Univ.

Experimental Setup

A polyurethane balloon was used to create 3-D motion for one of the mobile transceivers relative to the ground-based transceiver arrays (Figure 20). The balloon was sphere (diameter = 3m) and filled with helium (net-lift = 8.9kg). The balloon unit was either tethered to the ground or moved manually. The total weight of the payload was about 6.3+kg (Table 2). Each GPS transceiver unit consisted of a pseudolite (IntegriNautics IN200C) and a GPS receiver (CMC AllStar). 3% duty cycle RTCM pseudolite pulsing was inherited to mitigate near-far problems.

pseudolite	1.7 kg
GPS receiver	0.5 kg
wireless unit	0.3 kg
battery (12V)	1.4 kg
plastic box	0.9 kg
tether (nylon 40m)	1.5 kg
total	6.3+ kg

Table 2: Payload of aerial unit

A RHCP patch antenna was used for receiving and a linear dipole antenna for transmitting. Therefore, the range error due to the half cycle windups had to be taken into account every time the antennas of the balloon unit rotated horizontally with respect to the ground-based stationary transceivers. The transmitting-receiving antennas were vertically separated by 40 cm, which gave 40 dB or more isolation in between (Figure 21).

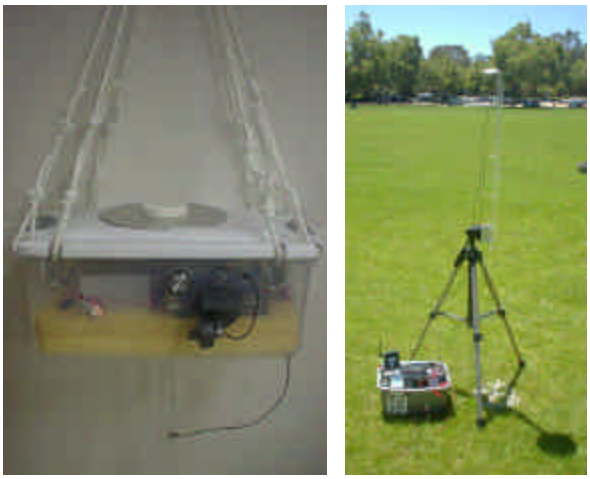

Figure 21: Antenna configuration : an aerial mobile XCVR (left) and a ground-based XCVR (right)

Test Results

Field demonstrations on the two configurations, Type A and Type B (Figures 10 and 12), were conducted to validate the above simulation results. Figure 22 shows the successful trial of the self-calibration by 2-D rover motion (Type A). The initial estimates of the stationary transceiver locations are given by the average of code measurements. The initial estimate of the trajectories of

the mobile units are calculated by the carrier phase range measurements with the integer biases initialized by code measurements. The stationary transceiver locations and the rover way points are precisely surveyed in advance by tape-measurement.

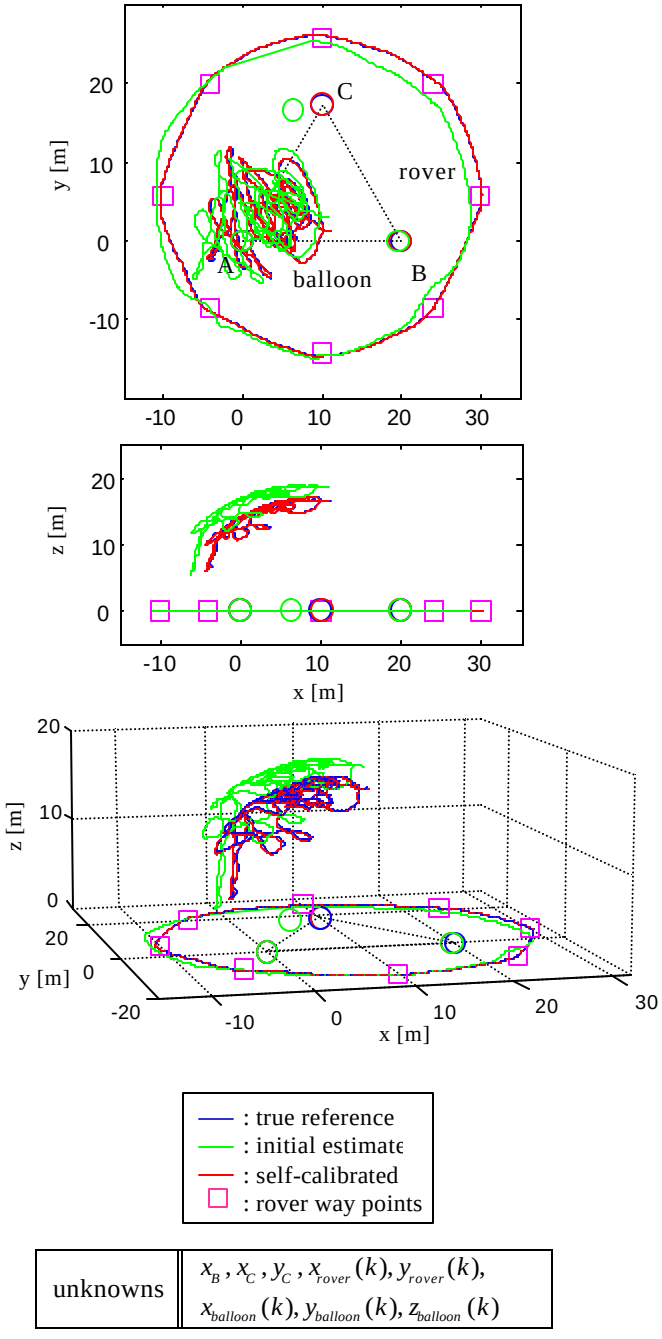

unknowns	$x_B, x_C, y_C, x_{rover}(k), y_{rover}(k),$ $x_{balloon}(k), y_{balloon}(k), z_{balloon}(k)$

Figure 22: Self-calibration by 2-D rover motion

As a result, the self-calibration process has successfully resolved both stationary array locations and rover-balloon trajectories by the rover motion around the stationary triangle array. The trajectories calculated with known stationary array locations were plotted as truth reference. The RMS errors from the true reference are 2.56 m for the initial estimates and 0.11 m for the self-calibrated solutions.

Figure 23 shows the test resuls from the field trials in the Type B configuration, but all the stationary transceivers are placed in a planar configuration on the ground. The balloon unit is moved manually up and down twice approximately from 10 m to 20 m during the circular horizontal motion. The initial estimates, the true reference, and the self-calibrated solutions are calculated in the same way described above.

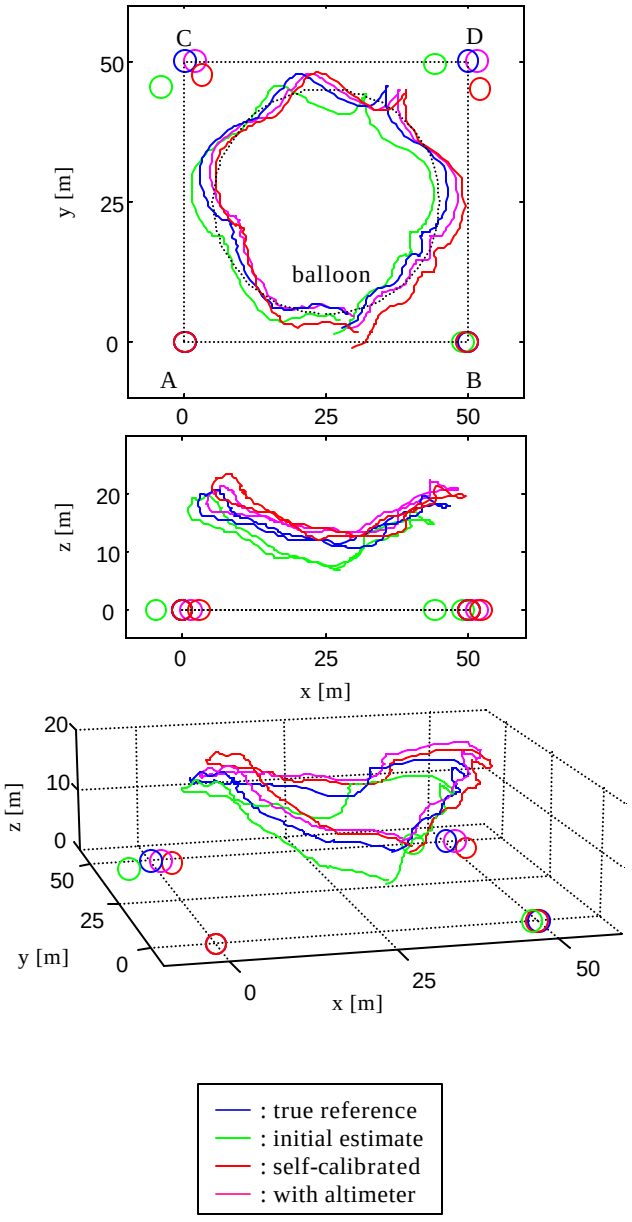

unknowns	$x_B, x_C, y_C, x_D, y_D, x_{balloon}(k), y_{balloon}(k), z_{balloon}(k)$

Figure 23: Self-calibration by balloon motion

Because of the poor geometry of the planar array, the self-calibrated trajectories have not converged close to the true reference. The solution with altimeter is also plotted in Figure 23, which is calculated by using altitude values from the true reference as known values in the self-calibration process. Compared with the self-calibrated trajectories, the solutions with altimeter have achieved much closer trajectories and stationary locations to the true reference. The residual errors in the solution with altimeter could be due to both the poor planar array geometry and the horizontal sensitivity of altitude uncertainty. The RMS errors from the true reference are 3.19 m for the initial estimates, 2.59 m for the self-calibrated solutions, and 1.12 m for the solution with altimeter.

CONCLUSIONS

The 3-D capabilities of GPS transcever arrays have been experimentally demonstrated and validated through the 3D-SCPA prototype with aerial transceiver units. The simulation results have shown that the self-calibration algorithm can apply to three-demensional positioning. The most important factor for the successful 3-D self-calibration is array geometry and motion-related change geometry. The planar arrays require extra out-of-plane units to provide better geometry to resolve 3-D positioning. In addition, vertical motions of mobile units are essential to achieve vertical observability to self-calibrate all the unknowns of interest. Furthermore, the potential advantage of sensor fusion with other dissimilar sensors has been discussed. To compensate for poor array geometry, altimeter measurements are integrated with GPS transceivers to aid the 3-D self-calibrations by providing explicit vertical information, although a certain amount of altimeter accuracy is necessary depending on the horizontal sensitivity of the altitude uncertainty.

ACKNOWLEDGEMENTS

This research has been conducted under NASA grants NCC2-1154 and NAG2-1464 as part of a joint effort between the Stanford University Aerospace Robotics Laboratory and the NASA Ames Research Center.

REFERENCES

[1] LeMaster, Edward, *Self-Calibrating Pseudolite Arrays: Theory and Experiment*, Ph.D. Thesis, Stanford University, May 2002.

[2] LeMaster, E., Matsuoka, M., Rock, S., "Field Demonstration of a Mars Navigation System Utilizing GPS Pseudolite Transceivers," *Proceedings of the 2002 IEEE Position, Location, and Navigation Symposium*, Palm Spring, CA, April 2002.

[3] Opshaug, G., "A Leapfrog Navigation System," *Proceedings of ION GPS-2002*, Portland, OR, September 2002.

[4] Parkinson, B., *et al*., *Global Positioning System: Theory and Applications, Vols. I & II*, American Institute of Aeronautics and Astronautics, 1996.

[5] Corazzini, T., How, J., "Onboard GPS Signal Augmentation for Spacecraft Formation Flying," *Proceedings of the ION GPS-98*, Nashville, TN, September 1998.

[6] Adams, John Carl, *Robust GPS Attitude Determination for Spacecraft*, Ph.D. Thesis, Stanford University, 2000.